Applied Chemical Engineering (2025) Volume 8 Issue 3 ISSN: 2578-2010 (O)
doi: 10.59429/ace.v8i3.5713

RESEARCH ARTICLE

Preparation and comparison of the performance of (CuO) nanostructures and (CuO)/(CdS) composites as anode electrodes in DSSCs using the natural dye of chard

Naseer Ali Badr*, Amer.M. J. Al-Shamari

College of Science, University of Kufa, College of Science, University of Kufa,Kufa, 540011, Iraq

***Corresponding author:** Naseer Ali Badr; naseera.almahdawi@student.uokufa.edu.iq

ABSTRACT

In this research, copper oxide (CuO) nanoparticles and copper oxide/cadmium sulfate (CuO/CdS) nanocomposite were prepared and used to construct dye-sensitized DSSCs, which were used as photoelectrodes using a natural dye prepared from chard as an adsorption medium (green dye) due to its low cost and availability in nature. The study indicated that the green dye performs better in DSSCs with CuO nanoparticles than in those with CuO/CdS nanocomposites, based on efficiency measurements using the Keithley apparatus. The power conversion efficiency (η) of CuO was 0.175%, while that of CdS was 0.141%. The current measured for both cells was 108.7 mA for CuO and 28.7 mA for CuO/CdS.

Keywords: Chemical synthesis; CuO; CuO/CdS; nanostructures; semiconductors; DSSCs; solar cell; transmission electron microscopy (TEM)

ARTICLE INFO

Received: 29 July 2025
Accepted: 21 August 2025
Available online: 31 August 2025

1. Introduction

A dye-sensitized solar cell is a key component for generating electricity without noise or pollution. Dye-sensitized cells are a promising alternative to currently available cells. Light energy is converted into electrical energy using an electrochemical process [1].

The basic components of a dye-sensitized cell are nanoparticles or extrinsic n-type semiconductors. An electrode and a photosensitive cell combine to form a semiconductor. The sensitizer absorbs light, and charge separation occurs at the conduction band surface. Redox electrolytes and counterelectrodes significantly influence the stability, efficiency, and performance of photovoltaic solar cells. A floating electrode is inserted into the electrolytic layer of a conventional dye-sensitized solar cell to create dye-sensitized tandem cells. These cells perform best in dimly lit and cloudy environments. Therefore, the development of nanostructured semiconductors, highly efficient sensitizers, and durable electrodes has made the performance of dye-sensitized solar cells more competitive [1, 2]. This review discusses current developments in new materials that can be used to create photovoltaic devices based on DSSCs with excellent performance [3,4,12]. In recent years, new designs for DSSCs have emerged using catalyst materials, and various redox shuttles are being studied, increasing their potential for integration into portable electronics, Internet of Things (IoT) devices, and wireless sensor networks [13].

Here, we synthesized CuO and (CuO/CdS) nanoparticles using a hydrothermal method, elucidating their structural, chemical, and optical properties and tracking their photovoltaic performance. Without the addition of copper oxide nanoparticles, a PCE of 1.12% was achieved for FTO solar cells. However, higher efficiencies of 1.75% and 1.41%, respectively, are achieved for CuO and CuO/CdS nanoparticles, effectively adding them to cells, due to efficient excitation generation, better light absorption, and photoexcited charge separation and collection. The concept of synthesizing CuO and CuO/CdS nanoparticles and using them in a photoactive mixture is a noteworthy contribution.

2. Experimental work

2.1. Synthesis of CuO of nanoparticles using the hydrothermal method

Copper oxide nanostructures can be easily and affordably produced using a hydrothermal method. Copper oxide nanoparticles were prepared using a hydrothermal method. After dissolving 0.1 M copper sulfate in 75 mL of deionized water, 0.2 M sodium hydroxide (NaOH) solution was added dropwise (approximately every 2 seconds) with vigorous stirring for 20 min. This resulted in a pH of 10.

After transferring the resulting solution to a 100 mL stainless steel autoclave, hydrothermal synthesis was performed for 8 h at approximately 160°C. The final product was dried at 70°C for 2 h [14]. The preparation process of the resulting compounds can be described below through the reactions [14].

$$CuSO_{4(aq.)} + 2\ NaOH_{(aq.)} \rightarrow Cu(OH)_2(s) + Na_2SO_{4(aq.)} \quad (2\text{-}1)$$

$$Cu(OH)_{2(s.)} + heat \rightarrow CuO_{(s.)} + H_2O_{(l.)} \quad (2\text{-}2)$$

Several have postulated the growth mechanism based on the experimental settings. Within the framework of our synthesis, we illustrate the CuO formation mechanism as follows: $Cu(OH)_2$ colloidal particles are created when copper sulfate solution is added to NaOH solution while being continuously stirred. During hydrothermal decomposition, a part of this colloidal $Cu(OH)_2$ dissolves into Cu^{2+} and OH^-, and it continues further to form $Cu(OH)_4^{-2}$. CuO nuclei form when their concentration reaches the supersaturation level [15].

2.2. Synthesis of CuO-CdS nanorod composites by the hydrothermal method

24 milliliters of ethanol solution were used to dissolve 0.1 milligrams of the prepared CdS nanorods. After 10 min. of stirring, $Cu(NO_3)_2.4H_2O$ was added to the aforesaid solution with an atomic ratio of Cd/Cu of 1/10. The solutions were then moved to a stainless steel autoclave walled for calcination, and the temperature was maintained at 160°C for 24 h. The sediment was separated by centrifugation an hour after it had cooled to room temperature. It was then repeatedly cleaned with ethanol and deionized water, and all samples were dried for two hours at 70°C in an oven [16].

2.3. Characterization of compounds prepared

2.3.1. X-Ray diffraction analysis

X-ray Diffraction (XRD) is a powerful analytical technique used to investigate the crystal structure, phase composition, and other structural parameters of materials. It works by analyzing the diffraction pattern produced when X-rays are directed at a sample. This pattern, essentially a fingerprint of the material, reveals information about the material's atomic arrangement and properties. XRD is based on the principle of Bragg's Law, which describes how X-rays are scattered by the regularly spaced atoms in a crystalline material, leading to constructive interference at specific angles. The interaction of X-rays with the crystalline structure generates a diffraction pattern, a unique "fingerprint" that can be used to identify the material's crystal structure, phase, and other properties.

XRD is widely used in various fields, including materials science, geology, chemistry, and pharmaceuticals, for texture analysis: Determining the preferred orientation of crystals in a material. Material characterization: Providing insights into the composition and structure of various materials, and Non-destructive Technique XRD is a nondestructive technique, meaning it doesn't fundamentally alter the sample during analysis. The XRD spectrum of CuO nanoparticles is displayed in **Figure 1**. The presence of both broad and sharp peaks makes it clear that a mixed phase of amorphous and crystalline states created the ensuing CuO products. Diffraction peaks at 2θ = 32.07°, 35.49°, 38.76°, 48.72°, 61.54°, and 66.09° are indicated on the JCPDS data card (89-2529). Correspond to the (110), (111), (200), (202), (113), and (311) crystal planes of cubic phase CuO. Using Debye-Scherer's equation, the CuO nanocrystals' crystallite size was calculated from an XRD spectrum peak with a higher intensity. The higher intensity plane of (111) has an average crystallite size of 35.74 nm [17]. numerous peaks. The average crystallite size (D) of CuO NPs was calculated from the Debye-Scherrer equation [18].

$$D = \frac{0.91\,\lambda}{\beta \cos\theta} \tag{2-1}$$

Where λ is the wavelength of X-ray transmittance, β is the full-width at half maximum (FWHM) in radians, and θ is the angle of diffraction. (λ = 0.15418 nm), and D is the crystallite size [19]. The crystallite size of the prepared copper oxide nanoparticles was of different sizes, ranging from 20 to 75 nm, which is suitable for the desired application. The crystallization of the copper oxide nanoparticle powder is cubic in shape, and the cubic shape is evidenced by the appearance of the diffraction peak in XRD at (200). The XRD results of the obtained copper oxide nanoparticles are consistent with the reported research. The narrow and strong diffraction peaks indicate the high crystalline quality of the copper oxide nanoparticle sample from the XRD data [17].

The CuO and CdS phases will be represented by characteristic peaks in the X-ray diffraction (XRD) patterns of CuO/CdS heterostructures. The exact peak positions and intensities will depend on the amounts of each element in the composite, as well as the crystal structures of CdS (often cubic or hexagonal) and CuO (monoclinic). The XRD patterns can be used to confirm the presence of both materials, determine their crystallinity, and estimate the diameters of the crystallites. CuO and CdS are present in the hybrid catalyst, as shown by the CuO-CdS as-prepared XRD pattern, which displays peaks for both the CuO and CdS phases. Peaks that are less intense than those of CuO and CdS are visible in the CuO-CdS diffractogram; this could be because CdS covers the CuO particle surface, causing crystal diffraction [20].

The (111), (200), (220), and (311) planes of the CuO and CdS phases are responsible for the broad peaks seen in the XRD patterns of CuO/CdS nanocomposites at 2θ values of 36.5, 43.38, 49.94, and 74. In particular, the (111) and (200) planes of CuO may be responsible for the peaks at 36.5 and 43.38, whereas the (220) and (311) planes of CdS, 2θ = 36.5, may be responsible for the peaks at 49.94 and 74. In its monoclinic structure, this peak is frequently linked to CuO (111) plane. Regarding 2θ = 43.38. This peak corresponds to CuO (200) plane, 2θ = 49.94. The (220) plane of CdS, which has a cubic structure, is responsible for this peak. 2θ is equal to 74. The (311) plane of CdS, which is also part of its cubic blende structure, is responsible for this peak. The broadness of the peaks indicates that there is some structural disorder and/or a relatively tiny crystallite size in the nanocomposites. This is a typical finding in nanomaterials, as depicted in **Figure 2** As attested by JCPDS Record No. 10-0454 and JCPDS File No. 80-1916 [21].

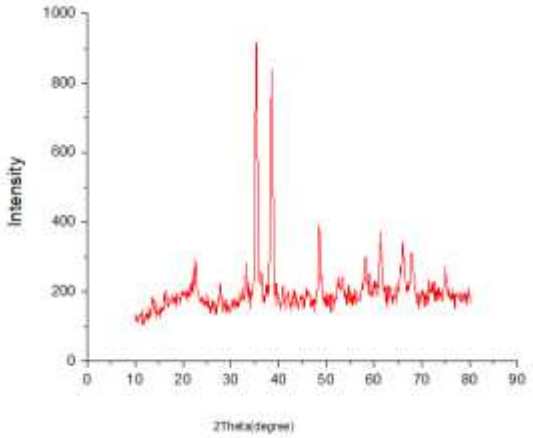

Figure 1. Shows the X-Ray Diffraction Analysis patterns of CuO nanoparticles

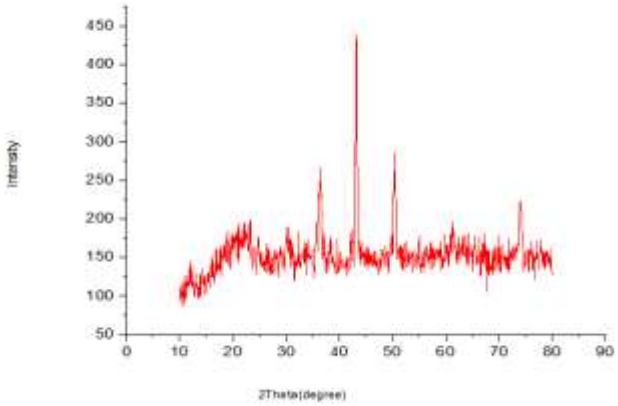

Figure 2. Shows the X-Ray Diffraction Analysis patterns of CuO-CdS nanocomposites

2.3.2. FE-SEM analysis

Figure 3 displays photographs of CuO nanoparticles as well as FE-SEM images of the nanostructures of the materials and nanocomposites created during the investigation (CuO, CuO/CdS). The normal diameter is 23.64 nm. **Figure 3** provides additional evidence that CuO forms as a tangle of regular-shaped nanoparticles.

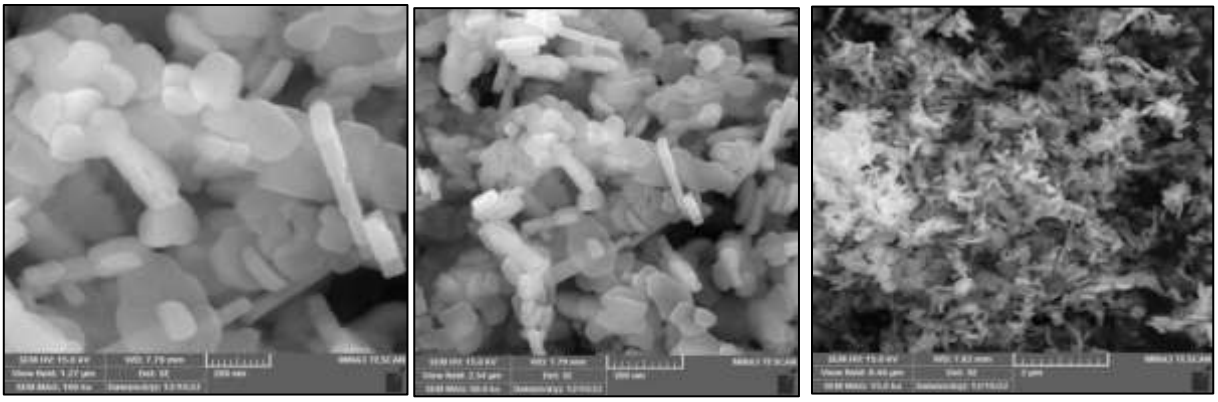

Figure 3. Shows images the field emission scanning electron microscope FE-SEM of CuO nanoparticles

Figure 4 shows a scanning electron microscope image (FE-SEM) of (CuO-CdS). The (CuO-CdS) appears irregular. The size ranges from (15.75 to75) nm. FE-SEM images indicated that most are occurring in aggregated form. In addition to the action of aqueous suspension, electrostatic forces are responsible for this agglomeration. This agrees with similar behavior to nanoparticle agglomeration in previous studies [22]. We notice that the spherical copper oxide (CuO) is distributed on the surfaces of the cadmium sulfide nanoparticles.

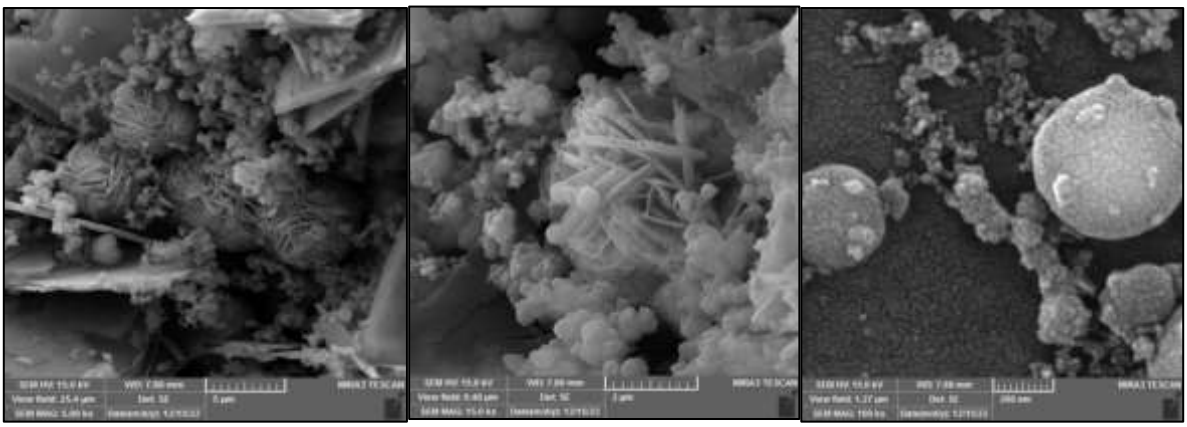

Figure 4. Shows images the field emission scanning electron microscope FE-SEM of CuO/CdS nanoparticles

2.3.3. TEM analysis

The produced nanoparticles and nanocomposite materials were assessed by TEM method analysis. CuO and CuO/CdS formations as shown in TEM pictures. The spherical shape of CuO nanoparticles, which range in size from (17.98 to 77.46) nm, is depicted in **Figure 5**.

The shapes and sizes of the CuO/CdS nanocomposite are displayed in **Figures 6**, and they range in size from (62.47 to 68.97) nm.

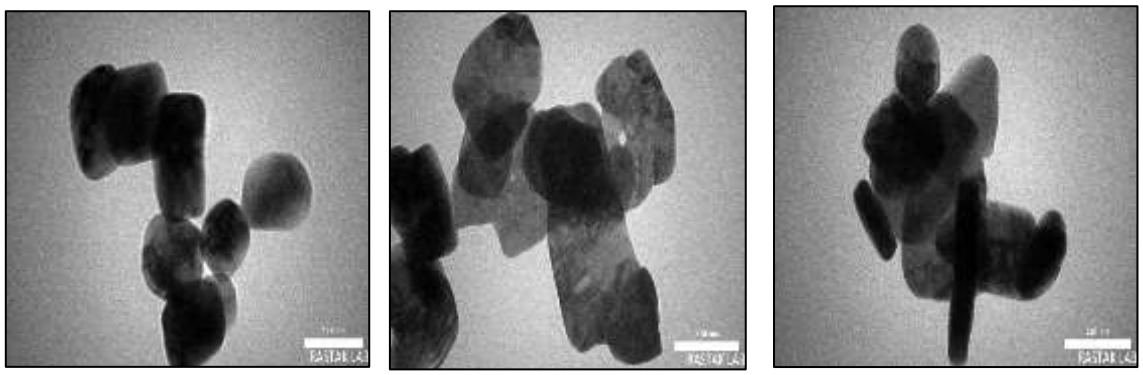

Figure 5. Shows images TEM of CuO nanoparticle

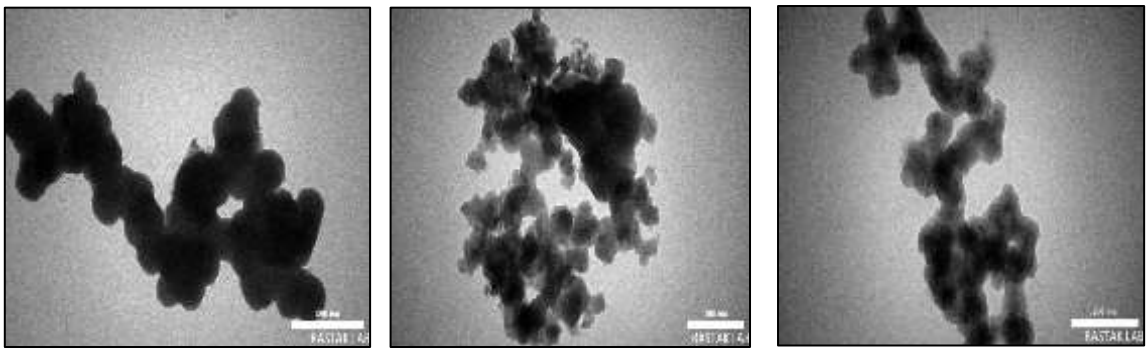

Figure 6. Shows images TEM of CuO-CdS nanocomposite

3. Fabrication of dye-sensitized solar cells

To create dye-sensitized solar cells, the study fabricated CuO and CuO/CdS nanoparticles and nanocomposites and used them as photo electrodes with a natural dye as an absorbing medium: green dye (from Swiss chard). **Figure 7** shows a DSSC working mechanism diagram and a schematic of the synthesis process using the natural dye and nanosurfaces. The findings demonstrated that the green dye enhanced the DSSCs' conversion efficiency (η), as displayed in **Table 1** with CuO surfaces compared to CuO/CdS surfaces. There are several reasons for this, one of which is the energy bandgap, which differs between the green dye and the surfaces. As a result, larger radial wavelengths are transmitted through the cells, where the dye absorbs it [23]. Secondly, because each surface area is unique, there exist variations in the surface areas of different nanomaterials. The efficiency of fabricated DSSCs increases with increased green dye absorption on the nanosurfaces. Furthermore, the present DSSC yield is a result of the elevated concentration of natural dye impurities. manufactured with green natural dye in the cells is reduced [24,25]. The low intensity of the light source used (22.54 mW/cm²) is an additional element causing the low current value of the manufactured DSSCs. Carbon is used as the cathode on the back surface of the FTO solar cell. Additionally, an iodine/iodide solution is used to form a conducting electrolyte. The photovoltaic performance, including the open-circuit voltage (V_{oc}), short-circuit current density (JSC), fill factor (FF), and power conversion efficiency (η), was measured using DSSCs made with a Keithley 2400. As a source measure, a xenon lamp with an illumination

intensity lower than (22.54 mW/cm²) (125 W) was used. The fill factor is calculated by dividing P_{max} by the sum of V_{oc} and I_{sc}. The ratio of P_{max} to the product of the input light irradiance (E) (Ac) and the solar cell surface area is used to compute the conversion efficiency.

$$FF = \frac{P_{Max}}{V_{oc} \times I_{SC}} \tag{1}$$

$$\eta = \frac{V_{oc} \times J_{SC} \times FF}{E} \tag{2}$$

$$FF = \frac{V_{Max} \times J_{Max}}{V_{oc} \times J_{SC}} \tag{3}$$

$$\%\eta = \frac{V_{oc} \times J_{SC} \times FF}{P_{in}} \tag{4}$$

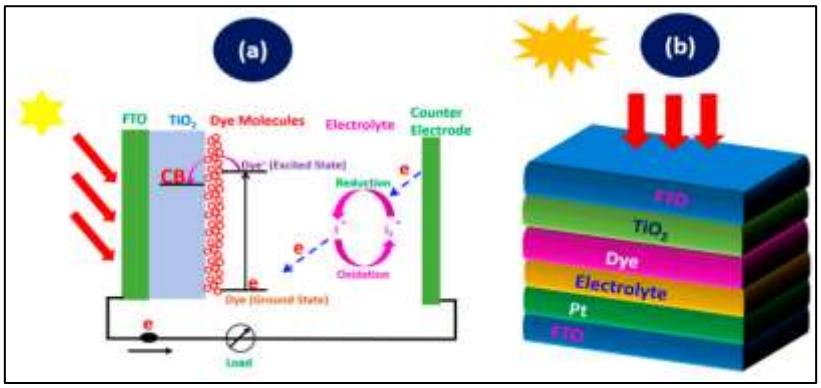

Figure 7. Working operation of a DSSC and (b) DSSC schematic diagram of the layers [26]

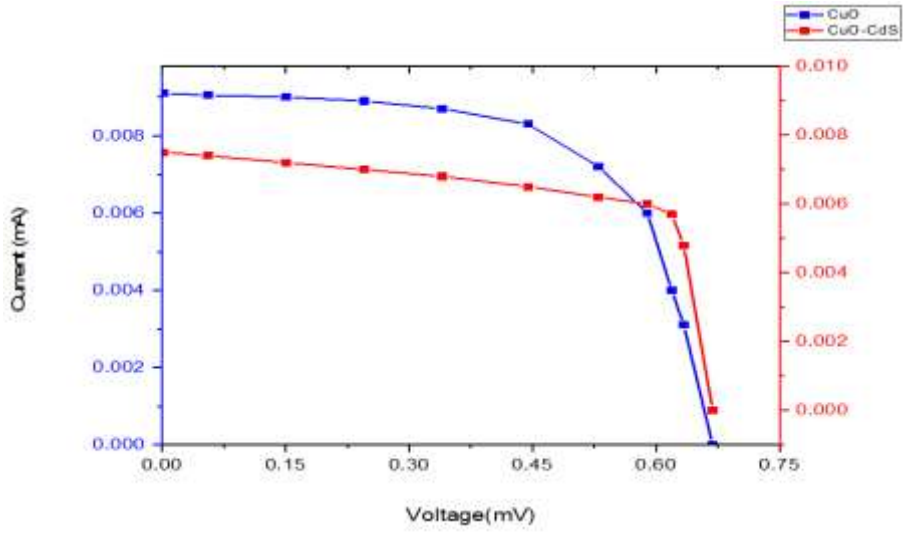

Figure 8. Shows the I–V properties of the nanoparticles and nanocomposite made from DSSCs and green dye (chard)

3.1. Prepare the anode electrodes

As previously mentioned, the hydrothermal technique is utilized to create nanomaterials in the hydrothermal method. The following steps are taken to create dye-stimulating solar cells (DSSCs): A very little amount of prepared nanomaterial is added to the prepared type (FTO) anode pole, which is made up of solar cells, and blended with ethyl alcohol and deionized water (DIW) and spread over the surface of the solar cell, leaving the cell's corners exposed with nanomaterial material. The solar cell is then placed in a warm oven (40–50°C) to dry sufficiently. After that, immerse it in the green dye solution to let it stick to the nanoscale

surface for 24 hours while it is dark. The solar cell is then removed and dried in the dark after that. Hence, we obtained the anode pole.

3.2. Preparation of the cathode electrodes

Without affecting the edges, carbon (graphite) is added to the solar cell's surface to prepare the cathode electrode. For this reason, the cathode pole was provided.

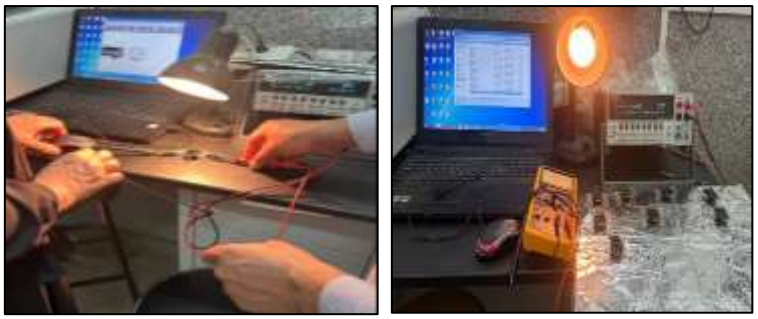

Figure 9. The solar cell and its shapes during the measurement of its efficiency with the Keithley device

Table 1. Shows the photo-electrochemical properties of DSSCs at a light intensity of 22.53 mW/cm² (A = 4.5 cm² green dye).

Catalyst / Dye		I_{SC} (mA)	V_{oc} (V)	I_{max} (mA)	V_{max} (V)	FF	η %
CuO	Green dye	1.088	83.6	1.14	69	0.865	0.175
CuO/CdS	Green dye	0.963	96.25	0.77	82.4	0.703	0.141

4. Conclusions

The effectiveness of nanomaterials (semiconductors) to create dye-sensitive cells (DSSCs), and because of their many surface area features, compact size, and energy output, solar cells are used in many aspects of daily life. Nanomaterials are produced using basic chemical techniques.

And she has green dye efficacy on dye-sensitive cells (DSSCs), as measured by conversion efficiency (η). Impact of the study's produced nanoparticles and nanocomposites (CuO, CuO/CdS) on the conversion efficiency (η) using the green dye (chard). The advantages of using various techniques to analyze the characteristics of nanomaterial surfaces and their effectiveness as photoelectrodes are significant.

Conflict of interest

The authors declare no conflict of interest

References

1. Yashwant Sawle, M. Thirunavukkarasu, "Chapter 9 - Techno-economic comparative assessment of an off-grid hybrid renewable energy system for electrification of remote area Author links open overlay panel. Design, Analysis, and Applications of Renewable Energy Systems Advances in Nonlinear Dynamics and Chaos (ANDC), 2021, Pages 199-247.
2. Suaad Abd M.A. Noor, Amer.M. J. Al-Shamari, "Preparation and comparison of the performance of ZnO and ZnO/MnO2 Nanostructures as anode electrodes in DSSCs", Indones. J. Chem., 2023, 23 (6), 1618 – 1626.
3. B. O'regan and M. Gr¨atzel, Nature, 1991, 353, 737–740.
4. M. K. Nazeeruddin, A. Kay, I. Rodicio, R. Humphry-Baker, E. Muller, P. Liska, N. Vlachopoulos and M. Gr ¨ ¨atzel, J. Am. Chem. Soc., 1993, 115, 6382–6390.
5. A. Hagfeldt and M. Gr¨atzel, Acc. Chem. Res., 2000, 33, 269– 277.
6. H. Pettersson, T. Gruszecki, L.-H. Johansson and P. Johander, Sol. Energy Mater. Sol. Cells, 2003, 77, 405–413.
7. Y. Chiba, A. Islam, Y. Watanabe, R. Komiya, N. Koide and L. Han, Jpn. J. Appl. Phys., 2006, 45, L638.
8. A. Yella, H.-W. Lee, H. N. Tsao, C. Yi, A. K. Chandiran, M. K. Nazeeruddin, E. W.-G. Diau, C.-Y. Yeh, S. M. Zakeeruddin and M. Gr¨atzel, Science, 2011, 334, 629–634.
9. K. Kakiage, Y. Aoyama, T. Yano, T. Otsuka, T. Kyomen, M. Unno and M. Hanaya, Chem. Commun., 2014, 50, 6379–6381.

10. S. Mathew, A. Yella, P. Gao, R. Humphry-Baker, B. F. E. Curchod, N. Ashari-Astani, I. Tavernelli, U. Rothlisberger, M. K. Nazeeruddin and M. Gr¨atzel, Nat. Chem., 2014, 6, 242–247.
11. K. Kakiage, Y. Aoyama, T. Yano, K. Oya, J. Fujisawa and M. Hanaya, Chem. Commun., 2015, 51, 15894–15897.
12. Y. Cao, Y. Liu, S. M. Zakeeruddin, A. Hagfeldt and M. Gr¨atzel, Joule, 2018, 2, 1108–1117.
13. H. Michaels, M. Rinderle, R. Freitag, I. Benesperi, T. Edvinsson, R. Socher, A. Gagliardi and M. Freitag, Chem. Sci., 2020, 11, 2895–2906.
14. Abd, M.A., R.M. Al-haddad, and K.H. Razeg, Synthesis and Characterization of copper oxide (II) nanoparticles prepared by hydrothermal process. Journal of University of Babylon for Pure and Applied Sciences, 2019. 27(4): p. 266-273.
15. Priyanka Marathey, Sakshum Khanna, Ranjan Pati, Indrajit Mukhopadhyay, Abhijit Ray, "Low temperature–controlled synthesis of hierarchical Cu2O/Cu(OH)2/CuO nanostructures for energy applications", Journal of Materials Research · August 2019,24 June 2019.
16. Nan Zhang, Xiaohui Ma, Yanyang Yin, Yu Chen, Chuannan Li, Jingzhi Yin, and Shengping Ruan, "Synthesis of CuO–CdS composite nanowires and their ultrasensitive ethanol sensing properties",Inorganic Chemistry Frontiers, Issue 1, 2019, 6, 238-247.
17. L. Ragunath1, J. Suresh, M. Sankaran, R. Suresh Kumar, A. I. Almansour and N. Arumugam, "SYNTHESIS AND CHARACTERIZATION OF COPPER OXIDE NANOPARTICLES USING RAMBUTAN PEEL EXTRACT VIA GREENER ROUTE ", Rasayan J. Chem., 14(4), 2660-2665(2021).
18. B. S. Hulbert and W. M. Kriven, "Specimen-displacement correction for powder X-ray diffraction in Debye–Scherrer geometry with a flat area detector," J. Appl. Crystallogr., vol. 56, no. 1, 2023.
19. C. C. Sun, A. H. You, and L. L. Teo, "XRD Measurement for Particle Size Analysis of PMMA Polymer Electrolytes with SiO2," Int. J. Technol., vol. 13, no. 6, pp. 1336–1343, 2022.
20. Mostafa Tarek, Kaykobad Md. Rezaul Karim, Sumaya Sarmin, Huei Ruey Ong, Hamidah Abdullah, Chin Kui Cheng, Md. Maksudur Rahman Khan "Photoelectrochemical activity of CuO-CdS heterostructured catalyst for CO2 reduction", Energy Security and Chemical Engineering Congress IOP Conf. Series: Materials Science and Engineering 736 (2020) 042023.
21. Zehraa Najim Abdul-Ameer, "ZnO/CuO/CdS Heterojunction Nanostructures as N-P-N for Optoelectronic Applications Effectiveness of Optoelectronic Devices" ,Iraqi Journal of Science, 2024, Vol. 65, No.5 , pp: 2460-2468.
22. Khalad A. AlMuhaysh, Antonis Sergis & Yannis Hardalupas, "Effects of pH and Nanoparticle Concentration on Al2O3–H2O Nanofluid Stability", International Journal of Thermophysics, Volume 46, article number 82, (2025)
23. P. Thickness, S. Plasmon, H. Jaafar, R. M. Rosnan, H. Yahaya, and S. S. Abdullah, "Enhancing Photocurrent Performance Based on DyeSensitized Solar Cells," vol. 12, no. 2111, pp. 1–14, 2019.
24. L. Schöttner, A. Nefedov, C. Yang, S. Heissler, and Y. Wang, "Structural Evolution of α -Fe 2 O 3 (0001) Surfaces Under Reduction Conditions Monitored by Infrared Spectroscopy Preview on Related Iron Oxide," Front. Chem., vol. 7, no. June, pp. 1–12, 2019.
25. D. Rangel, J. C. Gallegos, S. Vargas, F. García, and R. Rodríguez, "Optimized dye-sensitized solar cells: A comparative study with different dyes, mordants and construction parameters," Results Phys., vol. 12, no. November 2018, pp. 2026–2037, 2019.
26. Vijayakumar Paranthaman, Vijayakumar Paranthaman, K.S. Shalini Devi, K.B. Bhojanaa, V. Aravindan, Gurusamy Raman, Raju Suresh Kumar, Camellia Doroody, Reji Kumar Rajamony, Prajindra Sankar Krishnan, "Experimental and theoretical insights into enhanced light harvesting in dye-sensitized solar cells via Au@TiO2 core-shell and BaTiO3 nanoparticles", Journal of the Taiwan Institute of Chemical Engineers, Volume 165, December 2024, 105778.
27. Emeka Harrison Onah, N. L. Lethole 2, and P. Mukumb, "Luminescent Materials for Dye-Sensitized Solar Cells: Advances and Directions", Appl. Sci. 2024, 14, 9202.